JOURNAL OF PROPULSION AND POWER
Vol. 9, No. 6, Nov.–Dec. 1993

Computational Analysis of Vented Supersonic Exhaust Nozzles Using a Multiblock/Multizone Strategy

John R. Carlson* and S. Paul Pao†
NASA Langley Research Center, Hampton, Virginia 23681
and
Khaled S. Abdol-Hamid‡
Analytical Services and Materials, Inc., Hampton, Virginia 23681

A high-expansion ratio axisymmetric nozzle with and without longitudinal trailing-edge slots has been examined. Solutions were determined using a three-dimensional Navier-Stokes computer code. These results were compared with experimental data to determine the accuracy of the code for nozzle applications. Additionally, off-body flow physics were examined to understand the changes in nozzle performance with differing operating conditions. Highly overexpanded and near-design jet exhaust flows were simulated exhausting into subsonic and supersonic freestream Mach numbers. Pressure and velocity vector flowfields are shown and the predicted internal nozzle performance is compared with experimental data. Solutions were developed using laminar viscous stresses and thin-layer approximations.

Nomenclature

A_t = nozzle throat area, cm^2
F = total vector thrust, N
F_i = ideal isentropic gross thrust, N
f = incremental vector force of a computational cell
n = unit normal vector
p = static pressure, Pa
$p_{t,j}$ = jet total pressure, Pa
p_∞ = freestream static pressure, Pa
R = gas constant (γ = 1.4), 287.3 J/kg-K
r = reference length, cm
$T_{t,j}$ = jet total temperature, K
U = total velocity vector, m/s
w_i = ideal mass flow rate, kg/s
w_p = nozzle mass flow rate, kg/s
w_s = slot mass flow rate, kg/s
x = axial distance measured in the streamwise direction, cm
y^+ = nondimensional distance from wall in a turbulent shear layer
γ = ratio of specific heats
ρ = density, kg/m^3

Introduction

A SERIES of expendable, supersonic cruise (large expansion ratio) exhaust nozzle concepts for advanced applications were examined in a recent paper by Baker et al.[1] Several of these large expansion ratio, convergent-divergent nozzles were tested, and the results were reported by Baker et al.[2] These nozzle concepts have a fixed geometry and are optimized for a high nozzle pressure ratio (NPR) for operating at the design supersonic cruise Mach number and altitude. However, vehicles using these high expansion ratio nozzles while flying at subsonic speeds near sea level are operating these nozzles at pressure ratios far below the design point, and as a result experience significant loss in aeropropulsive performance. In order to improve the internal flow characteristics and performance at these speeds, divergent flap venting concepts were developed as described in Refs. 1 and 2. Both annular and longitudinal slots were considered. Performance measurements of a long shroud nozzle with an annular slot indicated significant performance improvements for low NPR (less than 10) operations. However, the performance was reduced by up to 1.5% for high NPR (greater than 20) operations. In any case, the performance did not exceed the measured performance of an unslotted short shroud nozzle configuration operating at similar conditions. The longitudinal slot configurations are expected to provide more open area, and thus higher mass flow, for venting at low NPR operations with fewer performance losses at the high NPR cruise conditions. Some of these configurations, such as the annular slot vented nozzle, have been analyzed using the PARC 2D/3D code using complex body-fitted grids.[3]

In this article, a multiblock/multizone Navier-Stokes code, PAB3D-v3, was applied to the analysis of the longitudinally slotted nozzle configuration. A photograph of the experimental model is shown in Fig. 1. An earlier version of this code, PAB3D-v2,[4] has demonstrated its effectiveness in computing three-dimensional jet exhaust plumes[5–8] and propulsion integration problems.[8,9] An algebraic grid generation code developed by Pao was used in these analyses. A surface fitted grid with a total of 14 blocks in five zones was generated for the nozzle configuration with a long shroud, concave centerbody, and longitudinal venting slots on the divergent flap. A total of 240,000 grid points were contained in the volume grid which covers one quadrant of the nozzle configuration by assuming symmetry at the quadrant boundaries. The PAB3D-v3 code includes options for different numerical schemes and turbulence models in solving the simplified form of the three-dimensional Navier-Stokes equations. It is designed to use multiblock/multizone grid structures for general aerodynamic applications. With the capability of modern supercomputers, the multiblock/multizone approach is preferred for handling very complex configurations. This approach greatly simplifies the process of grid generation for complex configurations by

Presented as Paper 91-0125 at the AIAA 29th Aerospace Sciences Meeting, Reno, NV, Jan. 7–10, 1991; received Aug. 31, 1992; revision received Feb. 16, 1993; accepted for publication May 3, 1993.

*Aerospace Engineer, Propulsion Aerodynamics Branch, Applied Aerodynamics Division. Senior Member AIAA.
†Aerospace Engineer, Propulsion Aerodynamics Branch, Applied Aerodynamics Division. Associate Fellow AIAA.
‡Senior Scientist. Member AIAA.

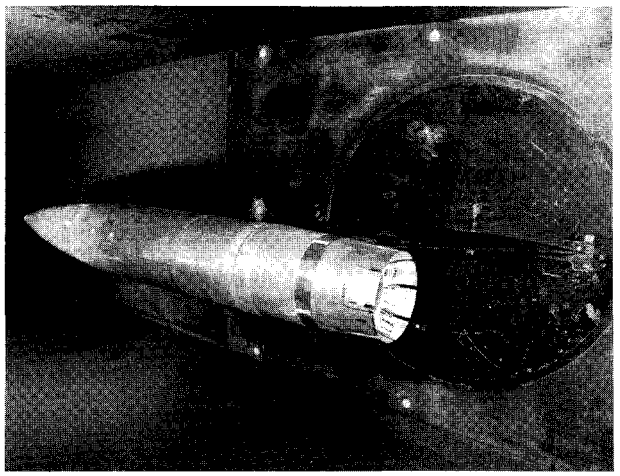

Fig. 1 Photograph of experimental model in wind tunnel.

allowing the separation of multiply connect regions into blocks, and by the flexibility of selecting grid topology and density in different blocks. In the case of PAB3D-v3, there is additional flexibility in being able to choose a different solver for each block to suit the particular flow conditions that may occur in a particular block. For example, a space marching algorithm can be used in a supersonic region for its greater computational efficiency, and a time-dependent solver can be used for subsonic or separated flow regions. In this article, computations were conducted employing mainly a time-dependent solver using the upwind flux difference splitting of Roe. The space marching solver was employed in a few occasions to speed up the rate of convergence for the overall solution. The PAB3D-v3 code also incorporated a nozzle performance prediction method developed by Carlson.[9] This method is used to predict the discharge coefficient and the internal thrust ratio for the nozzles in this study.

Governing Equations and Boundary Conditions

The governing equations are the Reynolds-averaged simplified Navier-Stokes equations obtained by neglecting all streamwise derivatives of the viscous terms. The resulting simplified Navier-Stokes equations are written in generalized coordinates and conservation form. The implementation of the full three-dimensional viscous stresses requires considerable resources, therefore, for the calculations the limitations of the thin-layer model had to be used. The PAB3D code allows different types of boundary conditions to be applied to segments of a given block face. For the present study solid walls are treated as no-slip adiabatic surfaces. The inflow boundary conditions used for the internal nozzle flow path are the total pressure and temperature. A boundary condition for Reimann invariants along the characteristics is specified for the freestream inflow face and the lateral freestream outer boundary of the flow domain. An extrapolation boundary condition was applied on the downstream outflow face where both the freestream and the nozzle plume stream exit the computational domain. Flow properties are transferred between block through the conservation of the mass and momentum fluxes across the block interface. Third-order continuity is maintained by the PAB3D code. However, some restriction on the multiblock grid is expected by the code, such as a simple multiple to one cell-to-cell correspondence at the block interface, and to maintain matched cell sizes in directions normal to the block interface.

It should be noted that only laminar viscous stresses are used in this study. Although several algebraic turbulence models are available in the PAB3D code, such models are not suitable for applications to free shear layers in general. For the present complex nozzle geometry, free shear layers are present at several locations within the nozzle interior and between the jet exhaust and external air downstream of the nozzle exit. On the other hand, boundary layers within the nozzle interior flow path, at this model scale, are expected to remain mostly laminar, based on the model length and flow velocities. Transition to turbulence may occur only on the downstream portion of the divergent flap. Similarly, the turbulence level is known to be very low in a supersonic jet mixing layer within the first few nozzle diameters downstream of the nozzle exit. This is particularly true for jet plumes exiting into a parallel supersonic freestream, which is the case for many of the conditions included in this study. Based on these assumptions, it is decided that the laminar viscous stress model should provide adequate simulation for the prescribed flow conditions in the study and provide an accurate picture of the global flow features that develop with this nozzle. In addition, the interpretation of the flow physics of the computed solutions can be better maintained by not using turbulence modeling techniques which may not be suitable for this study.

Computational Domain and Grid Generation

A surface fitted grid with a total of 14 blocks divided into five zones was generated for the longitudinally slotted nozzle configuration. This configuration had a long shroud, concave centerbody, and longitudinal venting slots on the divergent flap at eight equally spaced locations around the circumference of the nozzle. An unpublished compact grid generation code developed by Pao was used for grid generation. Both surface and volume grids were generated within this code by using transfinite interpolation.[10] Orthogonality at boundaries and smoothing, when necessary, were enforced by algebraic methods.

The computational domain included only one quadrant of the nozzle by assuming symmetry of flow variables at the quadrant boundaries. Two of the eight slots around the nozzle are included in this quadrant at 22.5- and 67.5-deg positions. The geometric symmetry of the nozzle could be described by a one-sixteenth definition. The implementation of a flow symmetry boundary condition for an arbitrarily oriented plane, i.e., boundaries not aligned with either the vertical x-z or x-y planes, was incomplete at the time of this study. The overall block structure, defined mainly by geometrical and flow break points, is shown in Fig. 2. Zones 1 and 2 cover the nozzle internal flow and external flow regions upstream of the tapered slots. The divergent flaps of the nozzle and the slots are included in zone 3. High grid density was used in the four blocks which are contiguous with the slots. Zone 4 was created to provide a grid density transition region from the fine grid around the nozzle to the coarser grid further downstream. The coarse grid in zone 5 extended approximately four nozzle exit radii downstream of the nozzle exit plane. A total of 240,000 points were contained in the grid for this nozzle. Fig. 3a shows a cross section of the three-dimensional grid in the middle of zone 3. A smooth transition of the circumferential grid spacing was provided between the

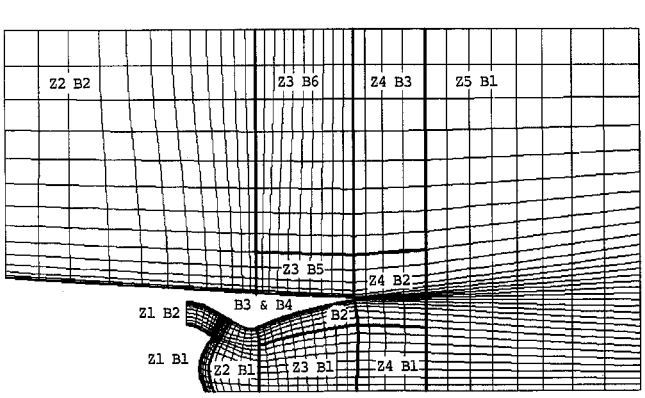

Fig. 2 Zone/block map for the slotted nozzle grid.

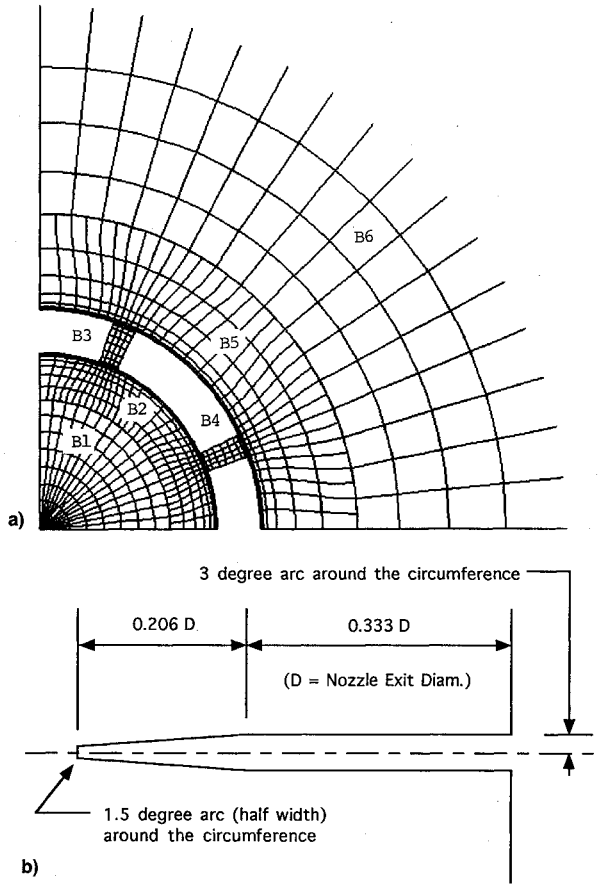

Fig. 3 Details of nozzle geometry: a) cross section of the grid in zone 3 and b) schematic for the tapered slot geometry.

nozzle wall, where the grid spacing is highly distorted, and the centerline or the freestream where equal spacing is maintained. Grid refinement from one block to another is also shown in Fig. 3.

Exact modeling of certain portions of experimental models may require the collapse of computational block faces to a single line or possibly a single point. Singular points or lines typically result in computational cell widths that are difficult to match to in the adjacent blocks without grid distortions or high grid stretching rates. The collapse of grid points along an axisymmetric centerline is not a problem, as that situation can be handled through the application of a flow symmetry boundary condition. Therefore, where necessary for maintaining a better grid quality, modifications are made in the geometric modeling to limit the degree of grid distortion and mismatch. Certainly consideration must be given as to the impact of some modifications in retaining the ability to predict the flow effects that are sought. In this investigation the shape of the tapered portion of the slot was modified. The minimum width of the upstream portion of the slot was made to be half the full width of the slot. This choice of widths, though seemingly arbitrary, was a compromise to prevent the collapsing of the upstream grid points of the slot block face. A top view of the tapered slot is shown in Fig. 3b. It is felt that the additional width of the slots will cause minimal change in the overall slot flow due to the nozzle wall thickness being large compared to the slot width along the upstream portion of the slot.

As part of the grid generation computer code package, the initial restart file for the flow solution was generated individually for each flow condition. A one-dimensional flow solution was computed within the nozzle according to the area ratio at each cross section. Initial conditions at the upstream face of each block were written to a separate file, as required by the PAB3D-v3 code. In zones 4 and 5, the initial jet plume shear layer and internal shock structures were established by making a single pass of space-marching calculation using the initial grid, initial conditions, and the PAB3D-v3 code.

Computational Method

In the present calculations, all blocks and zones used the upwind flux difference splitting in combination with a gradient limiting procedure to ensure monotonicity across discontinuities such as shock waves for calculating fluxes at cell interfaces. The computational scheme used is spatially third-order accurate throughout the entire computational domain and boundary surfaces. At some point during the computation, some of the blocks were turned off and the use of computer time was concentrated on iterations for the blocks with a large residual. In some situations, the space marching algorithm was used to speed up the convergence for the external and exit flow regions. With this flexibility, the total computational time was reduced by only working with the blocks or zones where special attention was needed to correct undesirable computational characteristics.

Performance Method

Nozzle performance was obtained through the application of the momentum theorem to a control volume surrounding the nozzle. The choice of surfaces over which the integration of forces is performed provides several different options for calculating the momentum and pressure forces on the nozzle. The method utilized for this investigation integrates the mass-flux and thrust force over the nozzle exit face and, when applicable, over the nozzle slots, using Eqs. (1) and (2):

$$w_p = \sum (\rho \boldsymbol{U} \cdot \boldsymbol{n}) \Delta A \tag{1}$$

$$\boldsymbol{F} = \sum [\rho \boldsymbol{U}(\boldsymbol{U} \cdot \boldsymbol{n}) + (p - p_\infty)\boldsymbol{n}] \Delta A \tag{2}$$

ΔA is the outflow area attributed to the incremental cell face, and $\boldsymbol{n}$ is the unit normal vector of the incremental cell.

Ideal mass-flow rate and thrust are determined from the isentropic flow equations, Eqs. (3) and (4) respectively, and are used to normalize the calculated mass-flow rate and thrust for comparisons with the experimental data:

$$w_i = \sqrt{\frac{\gamma}{R}} \left(\frac{2}{\gamma + 1} \right)^{\frac{\gamma+1}{2(\gamma-1)}} A_t \frac{p_{t,j}}{\sqrt{T_{t,j}}} \tag{3}$$

$$F_i = \sqrt{\frac{2\gamma R}{\gamma - 1}} w_p \sqrt{T_{t,j} \left[1 - \left(\frac{p_\infty}{p_{t,j}} \right)^{\frac{\gamma-1}{\gamma}} \right]} \tag{4}$$

Results and Discussion

In this article, six different cases of internal and external flow conditions were selected (Table 1) for flow and performance analysis of the slotted and unslotted long shroud nozzle with a concave centerbody.[2] The design NPR of this nozzle is 17.11, based on the geometrical expansion ratio of the configuration. Cases 1–4 are for the slotted nozzle, and cases 5 and 6 are for the axisymmetric (unslotted) nozzle operating at freestream Mach number 1.25 and NPR values of 5.01 and 11.63.

Each iteration required approximately 50 μs per grid point running on a Cray YMP computer. The core memory requirements for the PAB3D code is approximately 15 words per grid point for a typical grid. Even though the calculated residuals from the flow solver and the global features of the flowfield appeared to have changed little after 7 h of computer time, up to 15 h was sometimes required to obtain a flow solution acceptable for performance calculations. The standards for convergence of nozzle performance were as follows: less than 0.001 standard deviation in a plane-by-plane survey

Table 1 Long shroud nozzle test cases

Case	Configuration	M_∞	NPR	w_p/w_i		$F\text{-}D/F_i$	
				Experiment	Theory	Experiment	Theory
1	Slotted	0.0	19.88	0.936	0.938	0.9447	0.951
2	Slotted	1.253	5.01	—	0.940	—	0.801
3	Slotted	1.252	11.63	—	0.932	—	0.937
4	Slotted	2.500	16.89	0.931	0.933	0.9397	0.933
5	Unslotted	1.253	5.01	0.940	0.938	0.7563	0.775
6	Unslotted	1.253	11.63	0.938	0.933	0.9171	0.929

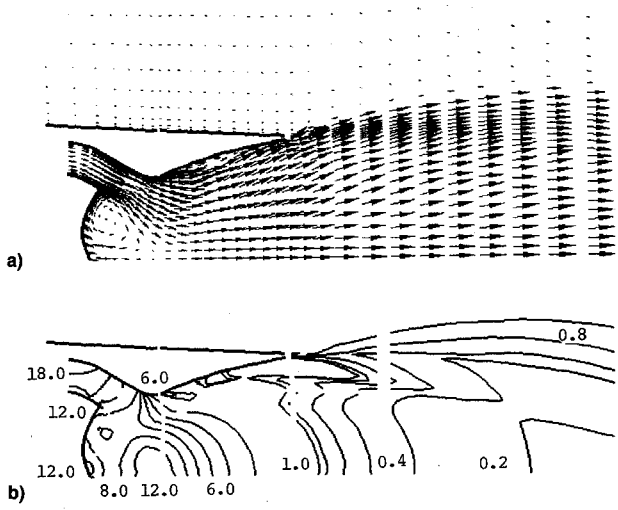

Fig. 4 Velocity vector and normalized static pressure distributions in the longitudinal plane of symmetry for the slotted nozzle operating at M = 0, and NPR = 19.88: a) velocity vectors shaded by values of Mach number and b) normalized static pressure distribution.

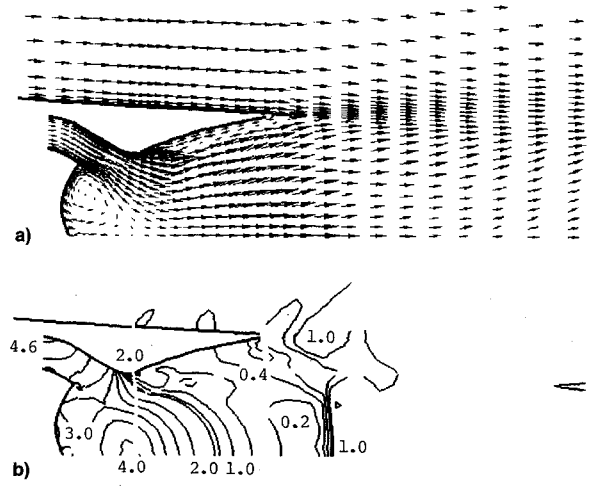

Fig. 5 Velocity vector and normalized static pressure distributions in the longitudinal plane of symmetry for the slotted nozzle operating at M = 1.25 and NPR = 5.007: a) velocity vectors shaded by values of Mach number and b) normalized static pressure distribution.

of mass flow in the nozzle. Ten planes in zone 1, block 2, were chosen for this survey in this set of calculations. Secondly, the thrust produced by the nozzle changed less than 0.1% for at least 500 iterations. In situations where an unsteady flow causes a regular fluctuation in the calculated thrust, an average value is computed from a statistical average over a few thousand iterations.

Flow Solutions

Results for case 1 (static freestream M = 0, NPR = 19.88) are shown in Figs. 4a and 4b. Figure 4a shows the velocity vectors shaded according to Mach number values. The nozzle flow is slightly underexpanded at these conditions where the flow expands smoothly, with the exception of two weak shock waves to the exit plane. In Fig. 4a, a large recirculation region was observed near the concave centerbody. The existence of the separated flow region is corroborated by previous calculations by Baker et al.,[1,2] and oil flow measurements on a similar configuration in recent soon to be published wind-tunnel tests at NASA Langley. For this operating condition, two shock surfaces are observed near the nozzle lip. The first surface is formed at the position where the exhaust flow exits the nozzle through the slots. The second surface is formed at the nozzle lip as a result of pressure differences at the nozzle exit. Figure 4b shows the pressure contours for the nozzle interior, the jet plume, and the freestream. The static pressure was initially 18 times the freestream static pressure at inflow boundary at the beginning of the annular channel around the centerbody, and expands to a pressure slightly higher than the freestream static pressure. The pressure jumps across the shock surfaces discussed above are relatively weak. The continuity and smoothness of both velocity vectors and the pressure contours across the block and zone boundaries indicate effective block-to-block and zone-to-zone communications.

Cases 2 and 3 have the same external Mach number of 1.25, and NPR values of 5.007 (overexpanded) and 11.63 (moderately overexpanded), respectively. The velocity vectors for these cases are shown in Figs. 5a and 6. Figures 5a and 6 show that a recirculation region is formed near the concave base very similar to the one found in case 1. For the NPR = 5.007 case, a large separated flow region is formed near the slots, as shown in Fig. 5a. A smaller, but similar region can be found in Fig. 6 for case 3 (NPR = 11.63). These separated flow regions are induced by the air mass flux through the slots into the nozzle. The flow characteristics for cases 2 and 3 are distinctly different from case 1 where the flow through the slot is in the opposite direction. As a result of the overexpanded flow condition internal to the nozzle, a Mach disk is formed close to the nozzle exit. The Mach disk is larger and closer to the nozzle exit for case 2 with NPR = 5.007 than for case 3 with NPR = 11.63. These operating conditions are expected to degrade nozzle performance. Figure 5b shows normalized static pressure contours for case 2. For all the grid blocks in the nozzle interior, the pressure distribution contours are qualitatively similar to those for case 1 as shown in Fig. 4b. This is expected from the fluid dynamics of convergent-divergent nozzles as long as the internal flow is not communicating directly with the external flow as a result of extensive regions of flow separation or by other phenomena.

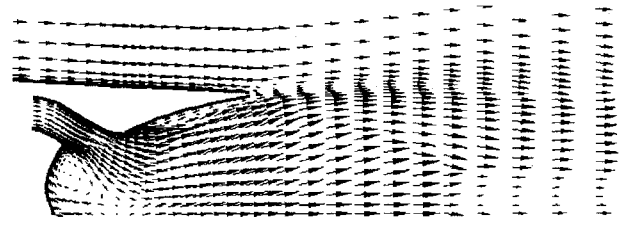

Fig. 6 Velocity vector distribution in the longitudinal plane of symmetry for the slotted nozzle operating at M = 1.25 and NPR = 11.63.

The last slotted case presented in this group has an external Mach number of 2.50 and NPR = 16.89, which are very close

to the conditions for which this nozzle was designed. Figure 7 shows the velocity vectors distribution for case 4. Two shock waves are initially formed near the exit of the nozzle, similar to case 1. However, these weak shocks merge into a single shock wave within a short distance downstream. Again, the internal flow in the convergent section of the nozzle is similar to the previous cases. A small Mach disk is formed at the end of the first shock cell. Its size, however, is much smaller than those found in cases 2 and 3.

The velocity vector distributions in the center plane of the slot for cases 1–4 are shown in Fig. 8. In each case, a recirculation region is formed close to the upstream end of the slot. However, this region varies in size and strength for different values of NPR. Case 1 shown in Fig. 8a, has the largest recirculating region and the exhaust flow starts to exit the nozzle at approximately 0.75 of the slot length. The lowest NPR case (Fig. 8b) has a strong recirculation zone inside the slot. The incoming airflow reaches the interior of the nozzle at approximately 0.30 of the slot length. The other transonic case (Fig. 8c) with NPR = 11.63 shows a weaker recirculation region inside the slot, and a smaller airflow through the slot into the nozzle.

Finally, Fig. 8d shows the Mach = 2.5 case which has the smallest airflow exchange through the slots. The external flow vectors are practically parallel to the wall of the afterbody. A small recirculation zone can be found just below the interior border of the slot.

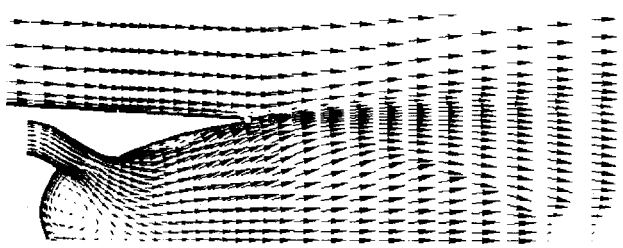

Fig. 7 Velocity vector distribution in the longitudinal plane of symmetry for the slotted nozzle operating at M = 2.50 and NPR = 16.89.

Nozzle Performance

An internal nozzle performance analysis for all six computed cases are shown in Figs. 9–11. Figure 9 shows the quantitative comparison of the ratio of slot mass flow with respect to the ideal nozzle mass flow for the different operating conditions. Figures 10 and 11 show comparisons between the calculated discharge coefficient and calculated nozzle thrust ratio with the available experimental data, respectively.

The degree of contribution to nozzle exit mass flow due to the slots is highly dependent on the nozzle pressure ratio. Operating conditions further from design induce more significant slot flows. Net inward slot flow occurs for conditions below design NPR, while net outward flow occurs for NPR above design, which is an expected result due to the pressure differences between external freestream and the internal nozzle flow at each condition. Up to a 10% contribution in exit mass flow is made by the slots for the nozzle operating at NPR = 5.0. The slots contribute less than 3% of the total mass into the nozzle for the transonic case at NPR = 11.63. For the cases operating close to design NPR (cases 1 and 4), the slots contribute little additional mass flow to the nozzle flow (less than 0.5%).

Agreement of computed and measured discharge coefficients (shown in Fig. 10) was within experimental accuracy (0.5% error) for the four cases with matching wind-tunnel data. Computed mass flow was relatively unchanged over the Mach number and NPR range as well as between the slotted and unslotted configurations.

The calculated thrust ratio was within 1.5% of the experimental data for NPR settings greater than 10 (design NPR = 17.11). Accurate modeling of the highly separated flow in the unslotted nozzle operating at NPR = 5 is difficult using the laminar viscous stresses. Laminar flow modeling would underpredict the degree of energy loss associated with turbulent flow. This, in conjunction with the extent of the flow separation, introduces a larger degree of error into the calculation. Unslotted nozzle performance was predicted high, possibly due to, as before, the laminar flow model in the flow solver. The slotted nozzle performance prediction, though, was typically low. Several different factors could contribute to this discrepancy. One factor, flow separation from the nozzle divergent flaps and subsequent flow development down-

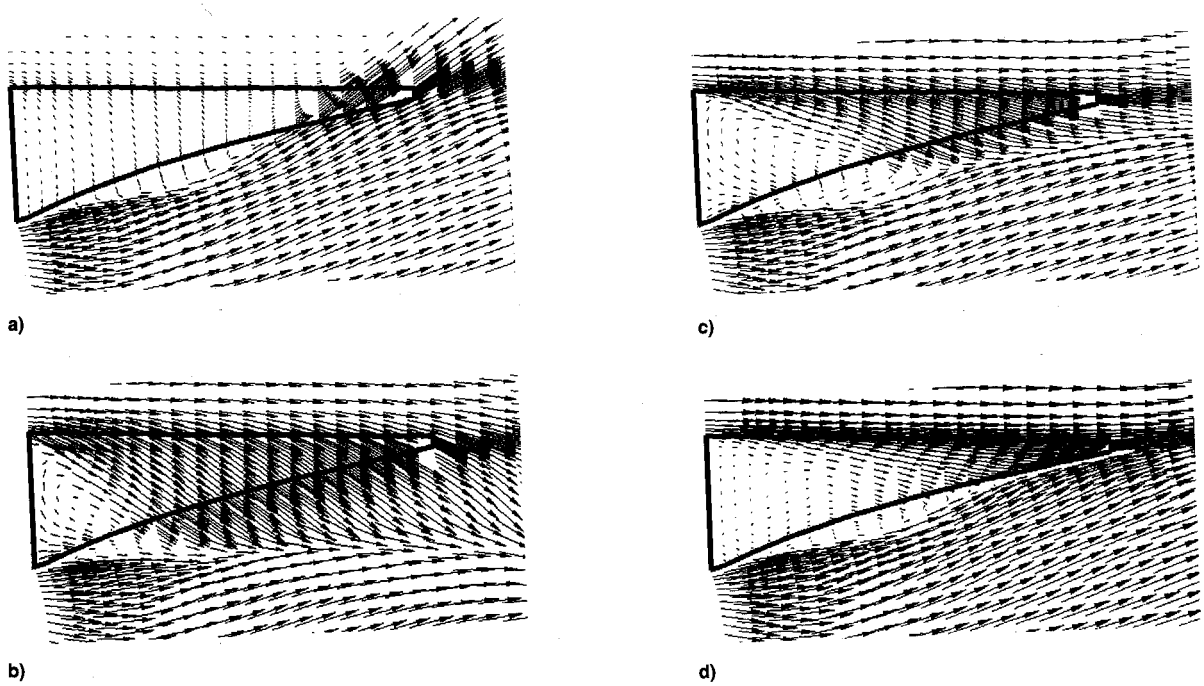

Fig. 8 Velocity vector distribution in the center plane of the slot at different values of Mach number and nozzle pressure ratio: a) case 1—M = 0, NPR = 19.88; b) case 2—M = 1.25, NPR = 5.007; c) case 3—M = 1.25, NPR = 11.63; and d) case 4—M = 2.50, NPR = 16.89.

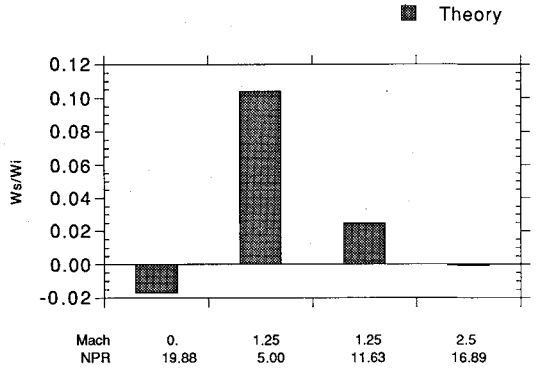

Fig. 9 Variation of normalized slot mass flow with Mach number and nozzle pressure ratio.

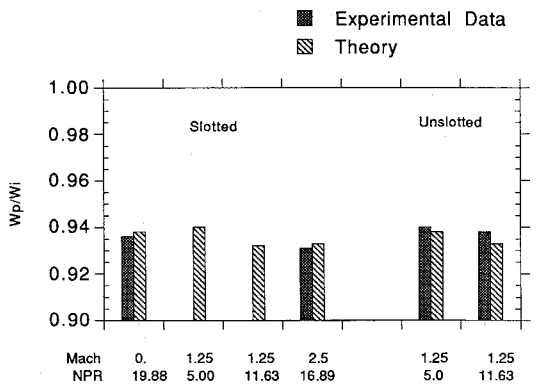

Fig. 10 Comparison of calculated nozzle discharge coefficient with experimental data for slotted and unslotted configurations.

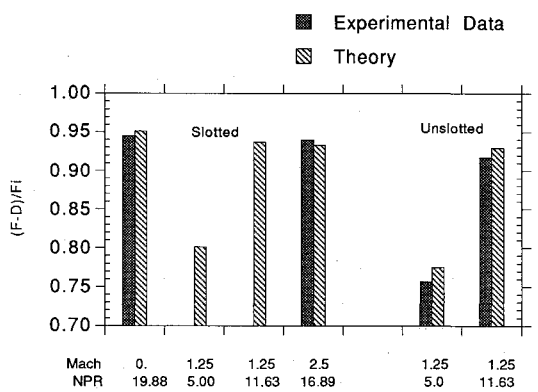

Fig. 11 Comparison of calculated thrust-minus-drag ratio with experimental data for slotted and unslotted configurations.

stream, significantly affects the nozzle performance. Calculated flow separation occurring upstream of the actual location could result in a smaller volume of effective momentum flux with a subsequent reduction in performance. An additional source of error could be the accuracy of modeling the recirculation in the slots affecting the predicted momentum lost or added due to the slots. Advanced turbulence models are expected to improve the ability to predict the effects of these regions of flow.

Concluding Remarks

Three-dimensional Navier-Stokes simulations have been made, using PAB3D-v3, for aerodynamic and performance predictions of slotted and unslotted nozzles. The range of flow conditions included nozzle pressure ratio values from 5 to 20 and freestream Mach numbers from 0 to 2.5. Nozzle flow with internal and external interactions including exhaust plume development were calculated using laminar viscous modeling. Large-scale flow effects such as flow separation, flow augmentation, and Mach disk formation were observed. Some small scale details of these effects may be different if proper turbulent flow modeling were used.

For all test cases, recirculation regions were predicted at different locations. A large recirculation region was detected near the concave base of the nozzle, and smaller regions were located near and around the slots. Mass flow through the slots was as high as 10% of the total mass flow in the nozzle. In general, discharge coefficient was predicted within 0.5%, and thrust ratio to within 1.5% of the measured values.

In the case of the unslotted nozzle operating at a transonic Mach number of 1.25, the thrust ratio drops to around 0.79 for a nozzle pressure ratio of 5.0. However, in the case of slotted nozzle, the thrust ratio is higher than 0.9 for all the cases simulated. For the transonic Mach number and nozzle pressure ratio of 5.0, an improvement of more than 10% in thrust ratio is gained by slotting the nozzle.

References

[1]Baker, V. D., Kwon, O., Vittal, B. V., and McKain, T. F., "Expendable Supersonic Exhaust Nozzle Concepts," AIAA Paper 89-2927, July 1989.

[2]Baker, V. D., Kwon, O., Vittal, B. V., Berrier, B., and Re, R., "Experimental Evaluation of Expendable Supersonic Nozzle Concepts," AIAA Paper 90-1904, Jan. 1990.

[3]Cooper, G. K., "The PARC Code: Theory and Usage," Arnold Engineering Development Center, AEDC TR-87-24, Oct. 1987.

[4]Abdol-Hamid, K. S., "Application of Multiblock/Multizone Code (PAB3D-v2) for the Three-Dimensional Navier-Stokes Equations: Preliminary Applications," NASA CR-182032, Sept. 1990.

[5]Abdol-Hamid, K. S., "The Application of 3D Space Marching Scheme for the Prediction of Supersonic Free Jets," AIAA Paper 89-2897, July 1989.

[6]Abdol-Hamid, K. S., and Compton, W. B., "Supersonic Navier-Stokes Simulations of Turbulent Afterbody Flows," AIAA Paper 89-2194, July 1989.

[7]Pao, S. P., and Abdol-Hamid, K. S., "Application of a New Adaptive Grid for Aerodynamic Predictions of Shock Containing Single Jets," AIAA Paper 90-2025, July 1990.

[8]Compton, W. B., Abdol-Hamid, K. S., and Abeyounis, W. K., "Comparison of Algebraic Turbulence Models for Afterbody Flows with Jet Exhaust," *AIAA Journal*, Vol. 30, No. 11, 1992, pp. 2716–2722.

[9]Carlson, J. R., "A Nozzle Internal Performance Prediction Method," NASA TP-3221, Oct. 1992.

[10]Eiseman, P. R., and Erlebacher, G., "Grid Generation for the Solution of Partial Differential Equations," Inst. for Computer Applications in Science and Engineering Rept. 87-57, NASA Langley Research Center, Hampton, VA, 1987.